Crystal Structure of a Synthetic High-Valent Complex with an $Fe_2(\mu\text{-}O)_2$ Diamond Core. Implications for the Core Structures of Methane Monooxygenase Intermediate Q and Ribonucleotide Reductase Intermediate X

Hua-Fen Hsu, Yanhong Dong, Lijin Shu, Victor G. Young, Jr., and Lawrence Que, Jr.*

Contribution from the Department of Chemistry and Center for Metals in Biocatalysis, University of Minnesota, 207 Pleasant Street SE, Minneapolis, Minnesota 55455

Received October 19, 1998

Abstract: In our efforts to model high-valent intermediates in the oxygen activation cycles of nonheme diiron enzymes such as methane monooxygenase (MMOH-**Q**) and ribonucleotide reductase (RNR R2-**X**), we have synthesized and spectroscopically characterized a series of bis(μ-oxo)diiron(III,IV) complexes, $[Fe_2(\mu\text{-}O)_2(L)_2](ClO_4)_3$, where L is tris(2-pyridylmethyl)amine (TPA) or its ring-alkylated derivatives. We now report the crystal structure of $[Fe_2(\mu\text{-}O)_2(5\text{-}Et_3\text{-}TPA)_2](ClO_4)_3$ (**2**), the first example of a structurally characterized reactive iron(IV)−oxo species, which provides accurate metrical parameters for the diamond core structure proposed for this series of complexes. Complex **2** has Fe−μ-O distances of 1.805(3) Å and 1.860(3) Å, an Fe−Fe distance of 2.683(1) Å, and an Fe−μ-O−Fe angle of 94.1(1)°. The EXAFS spectrum of **2** can be fit well with a combination of four shells: 1 O at 1.82 Å, 2−3 N at 2.03 Å, 1 Fe at 2.66 Å, and 7 C at 2.87 Å. The distances obtained are in very good agreement with the crystal structure data for **2**, though the coordination numbers for the first coordination sphere are underestimated. The EXAFS spectra of MMOH-**Q** and RNR R2-**X** contain features that match well with those of **2** (except for the multi-carbon shell at 2.87 Å arising from pyridyl carbons which are absent in the enzymes), suggesting that an $Fe_2(\mu\text{-}O)_2$ core may be a good candidate for the core structures of the enzyme intermediates. The implications of these studies are discussed.

Introduction

High-valent iron−oxo intermediates have been proposed in the dioxygen activation cycles of many heme and nonheme iron enzymes.[1] An iron(IV)−oxo porphyrin radical intermediate has been characterized for heme peroxidases and is proposed as the likely oxidant in the mechanisms of the cytochromes P450.[1a] High-valent intermediates have recently been identified for nonheme diiron enzymes such as methane monooxygenase (MMO) and ribonucleotide reductase (RNR).[1b,2] MMO catalyzes the hydroxylation of methane to methanol via a diiron(IV) intermediate **Q** formed in the hydroxylase component (MMOH-**Q**),[3] while RNR catalyzes the conversion of ribonucleotides to deoxyribonucleotides and utilizes an iron(III)iron(IV) intermediate **X** in its R2 subunit (RNR R2-**X**) to produce a tyrosyl radical that initiates this reaction.[4] Tandem rapid freeze quench Mössbauer and EXAFS studies on MMOH-**Q** and RNR R2-**X** reveal that these intermediates have diiron core structures with short Fe−O (1.8 Å) and Fe−Fe (2.5 Å) distances.[5,6] To account for such short Fe−Fe distances, it has been suggested that the diiron centers in these high-valent states must be bridged by at least two single atom bridges. Thus MMOH-**Q** and RNR R2-**X** are proposed to have $Fe_2(\mu\text{-}O)_2$ or $Fe_2(\mu\text{-}O)(\mu,\eta^1\text{-}O_2CR)$ core structures that stabilize these high-valent states.[5,6]

Synthetic models play a key role in bioinorganic chemistry, providing structural, spectroscopic, and mechanistic insights into the roles metal ions play in metalloenzymes. Thus, for oxygen activating metalloenzymes, there has been a significant effort to characterize high-valent complexes that may serve as the oxidizing intermediates in the mechanisms of these enzymes. In heme model chemistry, strong evidence has been obtained from spectroscopic and reactivity studies for oxoiron(IV) porphyrin and oxoiron(IV) porphyrin radical complexes,[7] but despite numerous attempts, no structure for a synthetic oxoiron(IV) porphyrin complex is yet available. We have proposed that the corresponding high-valent species in nonheme diiron enzymes have high-valent $Fe_2(\mu\text{-}O)_2$ cores,[8] a notion supported by precedents from synthetic manganese and copper chemistry

(1) (a) Sono, M.; Roach, M. P.; Coulter, E. D.; Dawson, J. H. *Chem. Rev.* **1996**, *96*, 2841−2887. (b) Wallar, B. J.; Lipscomb, J. D. *Chem. Rev.* **1996**, *96*, 2625−2658. (c) Que, L., Jr.; Ho, R. Y. N. *Chem. Rev.* **1996**, *96*, 2607−2624. (d) Kappock, T. J.; Caradonna, J. P. *Chem. Rev.* **1996**, *96*, 2659−2756.

(2) (a) Kurtz, D. M., Jr. *J. Biol. Inorg. Chem.* **1997**, *2*, 159−167. (b) Valentine, A. M.; Lippard, S. *J. Chem. Soc., Dalton Trans.* **1997**, 2925−3931. (c) Edmondson, D. E.; Huynh, B. H. *Inorg. Chim. Acta* **1996**, *252*, 399−404.

(3) (a) Lee, S.-K.; Nesheim, J. C.; Lipscomb, J. D. *J. Biol. Chem.* **1993**, *268*, 21569−21577. (b) Lee, S.-K.; Fox, B. G.; Froland, W. A.; Lipscomb, J. D.; Münck, E. *J. Am. Chem. Soc.* **1993**, *115*, 6450−6451. (c) Liu, K. E.; Valentine, A. M.; Wang, D.; Huynh, B. H.; Edmondson, D. E.; Salifoglou, A.; Lippard, S. J. *J. Am. Chem. Soc.* **1995**, *117*, 10174−10185.

(4) (a) Bollinger, J. M., Jr.; Edmondson, D. E.; Huynh, B. H.; Filley, J.; Norton, J.; Stubbe, J. *Science (Washington, D. C.)* **1991**, *253*, 292−298. (b) Ravi, N.; Bollinger, J. M., Jr.; Huynh, B. H.; Edmondson, D. E.; Stubbe, J. *J. Am. Chem. Soc.* **1994**, *116*, 8007−8014. (c) Sturgeon, B. E.; Burdi, D.; Chen, S.; Huynh, B.-H.; Edmondson, D. E.; Stubbe, J.; Hoffman, B. M. *J. Am. Chem. Soc.* **1996**, *118*, 7551−7557.

(5) Shu, L.; Nesheim, J. C.; Kauffmann, K.; Münck, E.; Lipscomb, J. D.; Que, L., Jr. *Science* **1997**, *275*, 515−518.

(6) Riggs-Gelasco, P. J.; Shu, L.; Chen, S.; Burdi, D.; Huynh, B. H.; Que, L., Jr.; Stubbe, J. *J. Am. Chem. Soc.* **1998**, *120*, 849−860.

(7) Meunier, B. *Chem. Rev.* **1992**, *92*, 1411−1456.

(8) (a) Que, L., Jr.; Dong, Y. *Acc. Chem. Res.* **1996**, *29*, 190−196. (b) Que, L., Jr. *J. Chem. Soc., Dalton Trans.* **1997**, 3933−3940.

10.1021/ja983666q CCC: $18.00
Published on Web 05/22/1999

which demonstrate that an $M_2(\mu\text{-}O)_2$ core can stabilize high oxidation states.[9] However, there are few examples of complexes with such $Fe_2(\mu\text{-}O)_2$ cores. Indeed the only crystallographically characterized complex prior to this report is the diiron(III) complex, $[Fe_2(\mu\text{-}O)_2(6\text{-}Me_3\text{-}TPA)_2](ClO_4)_2$ (**1**).[10,11] Higher valent derivatives of related complexes have been described, and they serve as the only synthetic models thus far that have spectroscopic and reactivity properties relevant to those of MMOH-**Q** and RNR R2-**X**.[12−14] In this paper, we report the crystal structure of $[Fe^{III}Fe^{IV}(\mu\text{-}O)_2(5\text{-}Et_3\text{-}TPA)_2](ClO_4)_3$ (**2**), the first example of a structurally characterized iron(IV)−oxo species capable of carrying out oxidation chemistry. This structure provides accurate metrical parameters for the $Fe_2(\mu\text{-}O)_2$ diamond core, which was first suggested by EXAFS analysis of its 5-methyl derivative $[Fe^{III}Fe^{IV}(\mu\text{-}O)_2(5\text{-}Me_3\text{-}TPA)_2](ClO_4)_3$ (**3**).[12] We have also analyzed its EXAFS spectrum and discuss implications for the diiron core structures of MMOH-**Q** and RNR R2-**X**.

Experimental Section

Materials. Reagents and solvents were purchased commercially and used as received. Complexes **1**−**3** were synthesized according to literature procedures.[10,12] *Caution! The perchlorate salts in this study are all potentially explosive and should be handled with care.*

Crystallographic Studies. Dark green crystals of **2** suitable for X-ray structure analysis were grown by layering methanol on top of a butanone solution of **2** at −80 °C. Data collection and analysis were conducted at the X-ray Crystallographic Laboratory of the Chemistry Department of the University of Minnesota. A crystal of **2** with dimensions 0.34 × 0.27 × 0.22 mm^3 was attached to a glass fiber and mounted on the Siemens SMART system for data collection at 173(2) K. An initial set of cell constants was calculated from reflections harvested from three sets of 20 frames. These initial sets of frames were oriented such that orthogonal wedges of reciprocal space were surveyed. This produced orientation matrices determined from 107 reflections. Final cell constants were calculated from a set of 8192 strong reflections. Additional crystallographic data and experimental conditions are summarized in Table 1. The structure was solved by direct methods.[15] All non-hydrogen atoms were refined with anisotropic displacement parameters. All hydrogen atoms were placed in ideal positions and refined as riding atoms with relative isotropic displacement parameters. Complete tables of atomic coordinates, bond lengths, and bond angles can be found in the Supporting Information.

X-ray Absorption Spectroscopy (XAS). XAS samples of the solid complexes were prepared individually as a 1:1 dispersion of the microcrystalline solid in boron nitride and kept cold with dry ice. XAS data were collected at beamline X9 of the National Synchrotron Light Source (NSLS) at Brookhaven National Laboratory. X-ray absorption spectra at the iron K-edge were collected between 6.9 and 8.0 keV as described previously,[16,17] and the monochromator was calibrated using the edge energy of iron foil at 7112.0 eV. The data were obtained in transmission mode ($A_{exp} = -\log I_t/I_0$) or fluorescence mode ($A_{exp}(C_f/C_0)$) at 10−20 K.

Table 1. Crystallographic Data of $[Fe_2(\mu\text{-}O)_2(5\text{-}Et_3\text{-}TPA)_2][ClO_4]_3$ (**2**)

	2·$2CH_3C(O)C_2H_5$·$1CH_3OH$
formula	$C_{57}H_{80}Cl_3Fe_2N_8O_{17}$
formula weight, amu	1367.34
space group	*C*2/*c*
a, Å	17.5143(2)
b, Å	18.7538(1)
c, Å	20.7147(2)
β, deg	111.945(1)
V, $Å^3$	6311.0(1)
Z	4
D(calcd), g cm^{-3}	1.439
temperature, K	173(2)
λ, Å	0.71073
μ, cm^{-1}	6.61
R^a ($I > 2\sigma(I) = 4328$)	0.0603
$R_w{}^b$	0.1465
goodness of fit	1.040

$^a R = \sum||F_o| - |F_c||/\sum|F_o|$. $^b R_w = (\sum[w(F_o^2 - F_c^2)^2]/\sum[wF_o^4])^{1/2}$.

The treatment of raw EXAFS data to yield χ is discussed in detail in review articles.[18,19] A modification of the EXAPLT program was employed to extract χ from A_{exp} by using a cubic spline function, including preliminary baseline correction and correction of fluorescence data for thickness effects and detector response.[16] The refinements reported were on $k^3\chi$ data, and the function minimized was $R = \{\sum k^6(\chi_c - \chi)^2/N\}^{1/2}$, where the sum is over N data points between 2 and 15 $Å^{-1}$.

Single-scattering EXAFS theory allows the total EXAFS spectrum to be described as the sum of shells of separately modeled atoms, e.g.

$$\chi_c = \sum nA[f(k)k^{-1}r^{-2}\exp(-2\sigma^2k^2)\sin(2kr + \alpha(k))]$$

where n is the number of atoms in the shell, $k = [8\pi^2m_e(E - E_0 + \Delta E)/h^2]^{1/2}$, and σ^2 is the Debye−Waller factor.[16] The amplitude reduction factor (A) and the shell-specific edge shift (ΔE) are empirical parameters that partially compensate for imperfections in the theoretical amplitude and phase functions.[20] Phase and amplitude functions were theoretically calculated using a curved-wave formalism.[21] A variation of FABM (fine adjustment based on models) was used here in the analysis procedure with theoretical phase and amplitude functions.[22] In each shell, two parameters were refined at one time (r and n or σ^2), while A and ΔE values were determined by using a series of crystallographically characterized model complexes. The fitting results indicate the average metal−ligand distances, the type and the number of scatterers, and the Debye−Waller factors which can be used to evaluate the distribution of Fe−ligand bond lengths in each shell. The EXAFS goodness of fit criterion applied here is

$$\epsilon^2 = [(N_{idp}/\nu)\sum(\chi_c - \chi)^2/\sigma^2]/N$$

as recommended by the International Committee on Standards and Criteria in EXAFS,[23,24] where ν is the number of degrees of freedom

(9) (a) Manchanda, R.; Brudvig, G. W.; Crabtree, R. H. *Coord. Chem. Rev.* **1995**, *144*, 1−38. (b) Tolman, W. B. *Acc. Chem. Res.* **1997**, *30*, 227−237.

(10) (a) Zang, Y.; Dong, Y.; Que, L., Jr.; Kauffmann, K.; Münck, E. *J. Am. Chem. Soc.* **1995**, *117*, 1169−1170. (b) Zheng, H.; Zang, Y.; Dong, Y.; V. G. Young, J.; Que, L., Jr. *J. Am. Chem. Soc.* **1999**, *121*, 2226−2235.

(11) Abbreviations used: 5-Et_3-TPA, tris(5-ethyl-2-pyridylmethyl)amine; 5-Me_3-TPA, tris(5-methyl-2-pyridylmethyl)amine; 6-Me_3-TPA, tris(6-methyl-2-pyridylmethyl)amine.

(12) Dong, Y.; Fujii, H.; Hendrich, M. P.; Leising, R. A.; Pan, G.; Randall, C. R.; Wilkinson, E. C.; Zang, Y.; Que, L., Jr.; Fox, B. G.; Kauffmann, K.; Münck, E. *J. Am. Chem. Soc.* **1995**, *117*, 2778−2792.

(13) (a) Dong, Y.; Que., L., Jr.; Kauffmann, K.; Münck, E. *J. Am. Chem. Soc.* **1995**, *117*, 11377-11378. (b) Dong, Y.; Zang, Y.; Shu, L.; Wilkinson, E. C.; Kauffmann, K.; Münck, E.; Que, L., Jr. *J. Am. Chem. Soc.* **1997**, *119*, 12683−12684.

(14) Kim, C.; Dong, Y.; Que, L., Jr. *J. Am. Chem. Soc.* **1997**, *119*, 3635−3636.

(15) Gilmore, C. J. *J. Appl. Crystallogr.* **1984**, *17*, 42−46.

(16) Scarrow, R. C.; Maroney, M. J.; Palmer, S. M.; Roe, A. L.; Que, L., Jr.; Salowe, S. P.; Stubbe, J. *J. Am. Chem. Soc.* **1987**, *109*, 7857−7864.

(17) Shu, L.; Chiou, Y.-M.; Orville, A. M.; Miller, M. A.; Lipscomb, J. D.; Que, L., Jr. *Biochemistry* **1995**, *34*, 6649−6659.

(18) Scott, R. A. *Methods Enzymol.* **1985**, *11*, 414−459.

(19) Teo, B.-K. *EXAFS Spectroscopy, Techniques and Applications*; Plenum: New York, 1981.

(20) Teo, B.-K.; Lee, P. A. *J. Am. Chem. Soc.* **1979**, *101*, 2815−2832.

(21) McKale, A. G.; Veal, B. W.; Paulikas, A. P.; Chan, S.-K.; Knapp, G. S. *J. Am. Chem. Soc.* **1988**, *110*, 3763−3768.

(22) Teo, B.-K.; Antonio, M. R.; Averill, B. A. *J. Am. Chem. Soc.* **1983**, *105*, 3751−3762.

(23) Bunker, G.; Hasnain, S. S.; Sayers, D.; Hasnain, S. S., Ed.; Ellis Horwood: New York, 1991; pp 751−770.

(24) Riggs-Gelasco, P. J.; Stemmler, T. L.; Penner-Hahn, J. E. *Coord. Chem. Rev.* **1995**, *144*, 245−286.

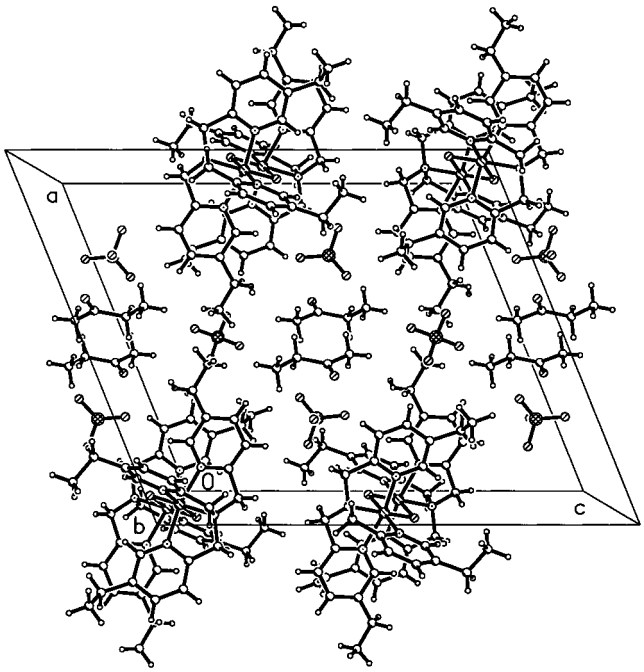

Figure 1. Crystal packing diagram for **2**.

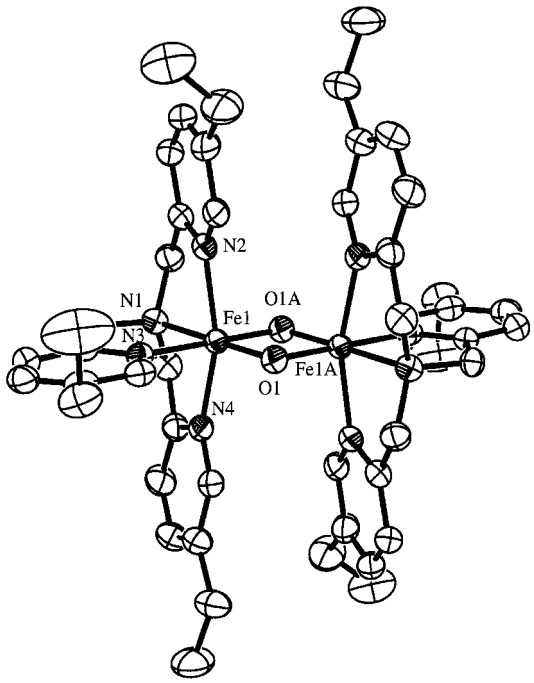

Figure 2. Thermal ellipsoid drawing of $[Fe(\mu\text{-}O)_2(5\text{-}Et_3\text{-}TPA)_2]^{3+}$ (**2**) showing 35% thermal ellipsoids. Hydrogen atoms have been omitted for clarity. Only one conformation of the disordered ethyl groups has been shown.

calculated as $\nu = N_{idp} - N_{var}$, N_{idp} is the number of independent data points, and N_{var} is the number of variables that are refined. N_{idp} is calculated as $N_{idp} = 2\Delta k\Delta R/\pi + 2$.[25] The use of ϵ^2 as the criterion for the goodness of fit allows us to compare fits using different numbers of variable parameters.

Results and Discussion

The series of $[Fe_2(\mu\text{-}O)_2L_2]^{3+}$ complexes with L being the tetradentate tripodal TPA ligand or ring-alkylated derivatives thereof are the only synthetic high-valent diiron complexes thus far[12−14] that serve as relevant models for the high-valent intermediates of nonheme diiron enzymes. Due to their thermal instability, such complexes have only been characterized at −40 °C or below and diffraction quality crystals have been difficult to obtain. The use of 5-Et_3-TPA has afforded a complex with somewhat higher thermal stability and, more importantly, solubility in a wider range of solvents. This development has finally allowed us to obtain a crystal structure of this novel complex.

Crystal Structure. Diffraction quality crystals of $[Fe_2(O)_2(5\text{-}Et_3\text{-}TPA)_2](ClO_4)_3$ (**2**) were obtained from butanone/methanol at −80 °C. The complex crystallizes with three solvent molecules, two of butanone and one of methanol. Importantly, the solvent butanone molecules form a tightly packed network that nicely fills the voids between the complex cation and anions (Figure 1). Crystals grown using acetone as solvent were more fragile and afforded a structure with an $R1$ of only 0.18.

A thermal ellipsoid drawing of the structure of the $[Fe_2(\mu\text{-}O)_2(5\text{-}Et_3\text{-}TPA)_2]$ (**2**) cation is shown in Figure 2, while selected bond lengths and angles are listed in Table 2. Complex **2** consists of a centrosymmetric $Fe_2(\mu\text{-}O)_2$ rhomb with the four nitrogen atoms of 5-Et_3-TPA completing the distorted octahedral coordination sphere of each iron center. The coordination environments of the two iron centers in **2** are identical, enforced by the inversion center. Despite the fact that **2** is formally an $Fe^{III}Fe^{IV}$ complex, there is no evidence for crystallographic disorder between the two iron atoms. This observation supports the description of **2** as a fully valence-delocalized mixed valence complex.[12]

Table 2. Selected Bond Lengths (Å) and Bond Angles (deg) for $[Fe_2(\mu\text{-}O)_2(5\text{-}Et_3\text{-}TPA)_2][ClO_4]_3$ (**2**)

Bond Distances (Å)			
Fe1−O1	1.805(3)	Fe1A−O1	1.860(3)
Fe1−N1	2.049(3)	Fe1−N2	2.003(3)
Fe1−N3	2.025(3)	Fe1−N4	2.025(3)
Fe1−Fe1A	2.683(1)	O−O1A	2.499(6)
Bond Angles (deg)			
Fe1−O1−Fe1A	94.1(1)	O1−Fe1−O1A	85.9(1)
O1−Fe1−N1	179.3(1)	O1−Fe1−N2	99.37(1)
O1−Fe1−N3	97.0(1)	O1−Fe1−N4	99.5(1)
O1A−Fe1−N1	93.4(1)	O1A−Fe1−N2	94.4(1)
O1A−Fe1−N3	176.9(1)	O1A−Fe1−N4	92.9(1)
N1−Fe1−N2	80.5(1)	N1−Fe1−N3	83.7(1)
N1−Fe1−N4	80.8(1)	N2−Fe1−N3	86.3(1)
N2−Fe1−N4	160.3(1)	N3−Fe1−N4	85.6(1)

The structure of **2** resembles that found for the bis(μ-oxo)-diiron(III) complex $[Fe_2(\mu\text{-}O)_2(6\text{-}Me_3\text{-}TPA)_2](ClO_4)_2$ (**1**),[10] and the two centrosymmetric core structures are compared in Figure 3. Complex **2** has Fe−μ-O bond lengths of 1.805(3) and 1.860-(3) Å, with the shorter Fe−O bond trans to the tertiary amine nitrogen of the TPA ligand and the longer Fe−O bond trans to a pyridine nitrogen. These bonds are respectively shorter than corresponding ones in **1** (1.841(1) and 1.917(4) Å), reflecting the higher oxidation state of the metal ions in **2**. The Fe−N distances of **2** range from 2.003(3) to 2.049(3) Å and average 2.026 Å, significantly shorter than those in **1** which average 2.24 Å.[10] As noted recently by Zang et al.,[26] this large difference stems mainly from the presence of the 6-methyl substituents in **1** and the resultant difference in spin states of the two diiron complexes. Complex **1** has been shown to be an antiferromagnetically coupled pair of high-spin iron(III) centers. In contrast, **2** is best described as a valence delocalized double exchange coupled low-spin iron(III)−low-spin iron(IV) pair, as indicated

(25) Stern, E. *Phys. Rev.* **1993**, *B 48*, 9825−9827.

(26) Zang, Y.; Kim, J.; Dong, Y.; Wilkinson, E. C.; Appelman, E. H.; Que, L., Jr. *J. Am. Chem. Soc.* **1997**, *119*, 4197−4205.

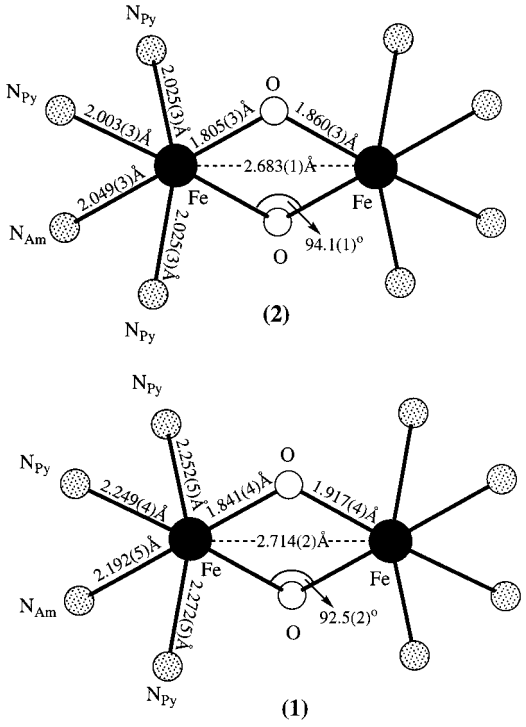

Figure 3. Core structural parameters of $[Fe_2(\mu\text{-}O)_2(5\text{-}Et_3\text{-}TPA)_2]^{3+}$ (**2**) and $[Fe_2(\mu\text{-}O)_2(6\text{-}Me_3\text{-}TPA)_2]^{2+}$ (**1**) from crystallographic data.

by its $S = {}^3/_2$ ground state and its sharp single Mössbauer quadrupole doublet.[12]

The distinct Fe−μ-O bond lengths of **2** ($\Delta r = 0.055$ Å) imparts a significant asymmetry on the $Fe_2(\mu\text{-}O)_2$ core. Interestingly, such a pronounced asymmetry does not occur in Mn_2O_2, Cu_2O_2, V_2O_2, and Cr_2O_2 complexes[27] (Table 4), even for the analogous but valence localized $[Mn^{III}Mn^{IV}(O)_2(TPA)_2]^{3+}$ whose Mn−O bonds differ in length by no more than 0.011 Å.[27b] This asymmetry of the Fe_2O_2 core is also observed for **1** ($\Delta r = 0.076$ Å),[10] as well as for $Fe^{III}_2(\mu\text{-}OH)_2$ complexes ($\Delta r = 0.075$ Å) and $Fe^{III}_2(\mu\text{-}OR)_2$ complexes ($\Delta r = 0.07$ Å).[28] Taken together, the Fe−μ-O bond asymmetry may be an intrinsic feature of the Fe_2O_2 rhomb.

Complex **2** has an Fe−Fe distance of 2.683(1) Å and an Fe−O−Fe angle of 94.1(1)°, core dimensions significantly different from those of diiron complexes with a single oxo bridge (2.95−3.57 Å and 115°−180°, respectively; Table 3).[29] Interestingly, its core dimensions are comparable to those of **1** (2.714(2) Å and 92.5(2)°, respectively), despite differences in oxidation and spin state (Figure 3). This limited flexibility of the $M_2(\mu\text{-}O)_2$ core is also observed in complexes with other first-row transition metal ions (Table 4).[27] For example, the M−M distance does not change significantly among $Mn^{III}Mn^{III}$, $Mn^{III}Mn^{IV}$, and $Mn^{IV}Mn^{IV}$ complexes, ranging from 2.64 to 2.75 Å, while the M−O−M angle varies from 93.9° to 99.5°. Indeed the Mn−Mn distance of $[Mn^{IV}_2(O)_2(Phen)_4]^{4+}$ (2.748(2) Å) is even longer than that of $[Mn^{III}Mn^{IV}(O)_2(Phen)_4]^{3+}$ (2.700(1) Å).[27a−d]

Complex **2** represents one of the few Fe^{IV} coordination complexes that are structurally characterized.[30] The paucity of available structures is presumably due to the reactivity of the Fe^{IV} oxidation state. Indeed, most of these structurally characterized Fe^{IV} complexes have several strongly electron donating ligands such as amidates or thiolates and are thus thermally stable. Complex **2** is an exception in that the only anionic ligands present are the two oxo bridges. As a consequence, it is stable only at −70 °C or below. At higher temperatures, it reacts with organic substrates and carries out the oxidation of phenols such as the diiron center in RNR R2 and the hydroxylation and desaturation of cumene, reactions analogous to those catalyzed by MMO and Δ9D, respectively.[14] Despite its reactivity, we have been able to crystallize **2**, and its structure is the first for a reactive iron(IV)−oxo species.

EXAFS Analysis. Prior to its crystallization, the structural parameters for the synthetic high-valent $Fe_2(\mu\text{-}O)_2$ core were determined from an EXAFS analysis of $[Fe_2(O)_2(5\text{-}Me_3\text{-}TPA)_2](ClO_4)_3$ (**3**).[12] An Fe−Fe distance of 2.89 Å was deduced from this earlier analysis, a value that is 0.2 Å longer than that determined for **2** from crystallography. To understand the basis for this discrepancy and to provide a means for interpreting the EXAFS-derived structures of the high-valent enzyme intermediates, MMOH-**Q** and RNR R2-**X**, we have obtained X-ray absorption spectra for **2** and analyzed the data in light of the crystal structure information. We have also analyzed the spectra of a number of related complexes whose crystal structures are available to support our findings.

The r'-space spectrum of **2** exhibits prominent features centered at $r' = 1.4$, 1.7, 2.1, and 2.4 Å, where r' corresponds to the actual metal−scatterer distance r after a phase shift correction of approximately 0.4 Å, i.e., $r \sim r' + 0.4$. The best fit to the k-space spectrum of **2** is shown in Figure 4, while the fitting protocol that led us to this best fit is summarized in Table 5. Single-shell fits of low-Z atoms for the first coordination sphere afforded Debye−Waller factors that were too large (fits 1 and 2 in Table 5), suggesting the need for a two-subshell fit. Indeed splitting the shell into two low-Z subshells at 1.82(1) and 2.00(1) Å (fits 3 and 4) resulted in acceptable Debye−Waller factors. These subshells correspond respectively to the

(27) (a) Goodson, P. A.; Oki, A. R.; Glerup, J.; Hodgson, D. J. *J. Am. Chem. Soc.* **1990**, *112*, 6248−6254. (b) Towle, D. K.; Botsford, C. A.; Hodgson, D. J. *Inorg. Chim. Acta* **1988**, *141*, 167−168. (c) Kitajima, N.; Singh, U. P.; Amagai, H.; Osawa, M.; Moro-oka, Y. *J. Am. Chem. Soc.* **1991**, *113*, 7757−7758. (d) Stebler, M.; Ludi, A.; Bürgi, H.-B. *Inorg. Chem.* **1986**, *25*, 4743−4750. (e) Mahapatra, S.; Halfen, J. A.; Wilkinson, E. C.; Pan, G.; Wang, X.; Young, V. G., Jr.; Cramer, C. J.; Que, L., Jr.; Tolman, W. B. *J. Am. Chem. Soc.* **1996**, *118*, 11555−11574. (f) Mahapatra, S.; Young, V. G., Jr.; Kaderli, S.; Zuberbühler, A. D.; Tolman, W. B. *Angew. Chem., Int. Ed. Engl.* **1997**, *36*, 130−133. (g) Mahadevan, V.; Hou, Z.; Cole, A. P.; Root, D. E.; Lal, T. K.; Solomom, E. I.; Stack, T. D. P. *J. Am. Chem. Soc.* **1997**, *119*, 11996-11997. (h) Duan, Z.; Schmidt, M.; Young, V. G., Jr.; Xie, X.; McCarley, R. E.; Verkade, J. G. *J. Am. Chem. Soc.* **1996**, *118*, 5302−5303. (i) Nishino, H.; Kochi, J. K. *Inorg. Chim. Acta* **1990**, *174*, 93−102.

(28) (a) Ou, C. C.; Lalancette, R. A.; Potenza, J. A.; Schugar, H. J. *J. Am. Chem. Soc.* **1978**, *100*, 2053−2057. (b) Thich, J. A.; Ou, C. C.; Powers, D.; Vasiliou, B.; Mastropaolo, D.; Potenza, J. A.; Schugar, H. J. *J. Am. Chem. Soc.* **1976**, *98*, 1425−1433. (c) Borer, L.; Thalken, L.; Ceccarelli, C.; Glick, M.; Zhang, J. H.; Reiff, W. M. *Inorg. Chem.* **1983**, *22*, 1719−1724. (d) Ménage, S.; Que, L., Jr. *Inorg. Chem.* **1990**, *29*, 4293−4297. (e) Walker, J. D.; Poli, R. *Inorg. Chem.* **1990**, *29*, 756−761. (f) Viswanathan, R.; Palaniandavar, M.; Prabakaran, P.; Muthiah, P. T. *Inorg. Chem.* **1998**, *37*, 3881−3884.

(29) Kurtz, D. M., Jr. *Chem. Rev.* **1990**, *90*, 585−606.

(30) (a) Caemelbecke, E. V.; Eill, S.; Autret, M.; Adamian, V. A.; Lex, J.; Gisselbrecht, J.-P.; Gross, M.; Vogel, E.; Kadish, K. M. *Inorg. Chem.* **1996**, *35*, 184−192. (b) Gerbelu, N. V.; Simonov, Y. A.; Arion, V. B.; Leovac, V. M.; Turta, K. I.; Indrichan, K. M.; Gradinaru, D. I.; Zavodnik, V. E.; Malinovskii, T. I. *Inorg. Chem.* **1992**, *31*, 3264−3268. (c) Vogel, E.; Will, S.; Tilling, A. S.; Neumann, L.; Lex, J.; Bill, E.; Trautwein, A. X.; Wieghardt, K. *Angew. Chem., Int. Ed. Engl.* **1994**, *33*, 731−735. (d) Knof, U.; Weyhermüller, T.; Wolter, T.; Wieghardt, K.; Bill, E.; Butzlaff, C.; Trautwein, A. X. *Angew. Chem., Int. Ed. Engl.* **1993**, *32*, 1635−1638. (e) Jüstel, T.; Weyhermüller, T.; Wieghardt, K.; Bill, E.; Lengen, M.; Trautwein, A. X.; Hildebrandt, P. *Angew. Chem. Int. Ed. Engl.* **1995**, *34*, 669−672. (f) Sellmann, D.; Geck, M.; Knoch, F.; Ritter, G.; Dengler, J. *J. Am. Chem. Soc.* **1991**, *113*, 3819−3828. (g) Sellmann, D.; Susanne, E.; Heinemann, F. W.; Knoch, F. *Angew. Chem., Int. Ed. Engl.* **1997**, *36*, 1201−1203. (h) Cummins, C. C.; Schrock, R. R. *Inorg. Chem.* **1994**, *33*, 395−396. (i) Kostka, K. L.; Fox, B. G.; Hendrich, M. P.; Collins, T. J.; Richard, C. E. F.; Wright, L. J.; Münck, E. *J. Am. Chem. Soc.* **1993**, *115*, 6746−6757.

Table 3. Summary of Core Structures of Selected Diiron Complexes

core structure	L[a]	Fe−Fe (Å)	Fe−μ-O(H)$_{av}$ (Å)	Fe−(OH)−Fe (deg)	ref
$Fe^{II}Fe^{III}(\mu\text{-OH})_3$	Me_3TACN	2.51	1.94	80.4	32a,b
$Fe^{III}Fe^{IV}(\mu\text{-O})_2$	5-Et_3-TPA	2.68	1.83	94.1	this work
$Fe^{III}_2(\mu\text{-O})_2$	6-Me_3-TPA	2.71	1.88	92.5	10a
$Fe^{III}_2(\mu\text{-O})(\mu\text{-OH})$	BPEEN	2.83	1.85 (μ-O)	100.2 (Fe−O−Fe)	10b
			1.98 (μ-OH)	91.1 (Fe−OH−Fe)	
	6-Me_3-TPA	2.91	1.82 (μ-O)[b]	106 (Fe−O−Fe)[b]	32
			1.99 (μ-OH)[b]	94 (Fe−OH−Fe)[b]	
$Fe^{III}_2(\mu\text{-OR})_2$	DBE, 3Cl, BHED	3.16−3.21	1.98−2.00	103.7−107.4	28d−f
$Fe^{III}_2(\mu\text{-O})(\mu\text{-H}_3O_2)$	TPA, 5Et_3-TPA	3.35−3.39	1.80−1.81	136−139	12
$Fe^{III}_2(\mu\text{-O})$	TPA	3.57	1.79	174	12
$Fe^{III}_2(\mu\text{-OH})_2$	DPD, DIPIC, CHEL, BHED	3.08−3.16	1.96−2.02	102.8−105.3	28a−c

[a] Me_3TACN = 1,4,7-trimethyl-1,4,7-triazacyclononane; DBE = 2-[bis(2-benzimidazolylmethyl)amino]ethanol; BHED = 1,2-bis(2′-hydroxybenzyl)ethane-1,2-diamine; DPD = 4-(dimethylamino)-2,6-pyridinedicarboxylate; DIPIC = 2, 6-pyridinedicarboxylate; CHEL = 4-hydroxo-2,6-pyridinedicarboxylate. [b] The structural parameters reported here are deduced from EXAFS analysis due to disorder of the $Fe^{III}_2(\mu\text{-O})(\mu\text{-OH})$ core in the crystal structure.

Table 4. Crystal Structure Parameters for $[M_2(\mu\text{-O})_2L_2]$ Complexes

core structure	L[a]	M−M (Å)	M−O−M (deg)	M−O (Å)	ref
$Fe^{III}Fe^{IV}(\mu\text{-O})_2$	5-Et_3-TPA	2.683(1)	94.07(1)	1.805(3), 1.860(3)	this work
$Fe^{III}_2(\mu\text{-O})_2$	6-Me_3-TPA	2.714(2)	92.5(2)	1.841(4), 1.917(4)	10a
$Mn^{III}_2(\mu\text{-O})_2$	6-Me_2-TPA	2.674(4)	93.9(3)	1.818(9), 1.841(6)	27a
$Mn^{III}Mn^{IV}(\mu\text{-O})_2$	TPA	2.643(1)		1.771(3), 1.782(3)	27b
				1.835(3), 1.839(3)	
$Mn^{III}_2(\mu\text{-O})_2$	Tp^{ipr_2}	2.696(2)	96.5(3)	1.787(6), 1.806(5)	27c
			97.0(3)	1.808(6), 1.813(6)	
$Mn^{III}Mn^{IV}_2(\mu\text{-O})_2$	$Phen_2$	2.700(1)	96.0(1)	1.808(3), 1.820(3)	27d
$Mn^{IV}_2(\mu\text{-O})_2$	$Phen_2$	2.748(2)	99.5(2)	1.797(3), 1.798(3)	27d
				1.798(3), 1.805(3)	
$Cu^{III}_2(\mu\text{-O})_2$	Bn_3TACN	2.794(2)	101.4(2)	1.808(5), 1.803(5)	27e
$Cu^{III}_2(\mu\text{-O})_2$	$^{i}Pr_4$dtne/2	2.783(1)	99.0	1.823(4), 1.824(4)	27f
			99.3	1.827(4), 1.836(4)	
$Cu^{III}_2(\mu\text{-O})_2$	MECD	2.743(1)	98.9	1.814(6), 1.809(6)	27g
				1.796(6), 1.804(6)	
$V^{IV}_2(\mu\text{-O})_2$	$[N(SiMe_3)_2]_2$	2.612(2)	92.9(2)	1.802(4)	27h
$Cr^{V}_2(\mu\text{-O})_2$	PFP	2.628(2)	92.4(2)	1.806(5), 1.818(5)	27i

[a] Tp^{ipr_2} = hydrotris(3,5-diisopropyl-1-pyrazolyl)borate; Phen = 1,10-phenanthroline; Bn_3TACN= *N*,*N*′,*N*″-tribenzyl-1,4,7-triazacyclononane; $^{i}Pr_4$dtne = 1,2-bis(4,7-diisopropyl-1,4,7-triaza-1-cyclononyl)ethane; PFP = perfluoropinacolate; MECD = *N*,*N*′-dimethyl-*N*,*N*′-diethylcyclohexanediamine.

Table 5. EXAFS Fits for $[Fe_2(\mu\text{-O})_2(5\text{-}Et_3\text{-TPA})_2][ClO_4]_3$ and $[Fe_2(\mu\text{-O})_2(5\text{-}Me_3\text{-TPA})_2][ClO_4]_3$

	Fe−N/O			Fe−N/O			Fe−Fe			Fe−C				
fit	*n*	*r* (Å)	σ^{2a}	*n*	*r* (Å)	σ^{2a}	*n*	*r* (Å)	σ^{2a}	*n*	*r* (Å)	σ^{2a}	$(\epsilon^2 \times 10^4)^b$	$(\epsilon^2 \times 10^4)^c$
							$[Fe_2(\mu\text{-O})_2(5\text{-}Et_3\text{-TPA})_2][ClO_4]_3$[d]							
1	6	1.91	22										9	
2	5	1.91	18										5	
3	1	1.80	4.1	4	1.99	9.3							8	
4	1	1.82	0.5	3	2.00	4.5							5	33
5	1	1.83	−0.9	3	2.00	3.2	1	2.92	7.8					27
6	1	1.82	−0.7	3	2.00	3.4				6	2.93	6.5		35
7	1	1.83	−0.5	3	3.00	3.5	1	2.92	7.5	6	2.63	3.2		37
8	1	1.82	−0.7	3	2.00	3.2	1	2.61	6.5	7	2.87	3.6		18
9	1	1.83	−2	2	2.01	0	1	2.61	6	8	2.87	5		12
							$[Fe_2(\mu\text{-O})_2(5\text{-}Me_3\text{-TPA})_2][ClO_4]_3$[e]							
A	1	1.81	−2	3	2.00	1	1	2.60	5	7	2.87	4		9
B	1	1.82	0	2	2.00	3	1	2.59	9	7	2.89	6		6

[a] σ^2 is in units Å$^2 \times 10^3$. [b] Back-transformation range 0.8−1.9 Å. [c] Back-transform range 0.8-2.65 Å. [d] Fits 1−9 are for the same sampe (k = 2−14.5 Å^{-1}). [e] Fits A and B are best fits for two individual samples (k = 2−14.5 Å^{-1} for A and 2−13 Å^{-1} for B).

oxo bridges and nitrogen ligands of the complex, in excellent agreement with the crystallographic values of 1.83 (Fe−μ-O$_{av}$) and 2.03 Å (Fe−N$_{av}$) found for **2**. However, the coordination numbers are somewhat underestimated, particularly for the 1.8 Å subshell, presumably due to destructive interference effects among the components of the first coordination sphere. Of these fits, fit 4 was chosen for further fits of the outer-sphere parameters because it has the best goodness-of-fit value. Furthermore, the low Debye−Waller factor associated with the 1.8 Å shell is typical of oxo bridges in the diiron(III) complexes we have studied.[16]

We have previously noted the large intensity of the outer-sphere features, which must arise from an outer-sphere scatterer or scatterers with little vibrational disorder. Such intense outer-sphere features have been observed in other complexes with M_2O_2 cores and have been useful for identification of such cores

(31) (a) Yachandra, V. K.; Sauer, K.; Klein, M. P. *Chem. Rev.* **1996**, *96*, 2927−2950. (b) Yachandra, V. K.; DeRose, V. J.; Latimer, M. J.; Mukerji, I.; Sauer, K.; Klein, M. P. *Science* **1993**, *260*, 675−679. (c) Waldo, G. S.; Yu, S.; Penner-Hahn, J. E. *J. Am. Chem. Soc.* **1992**, *114*, 5869−5870.

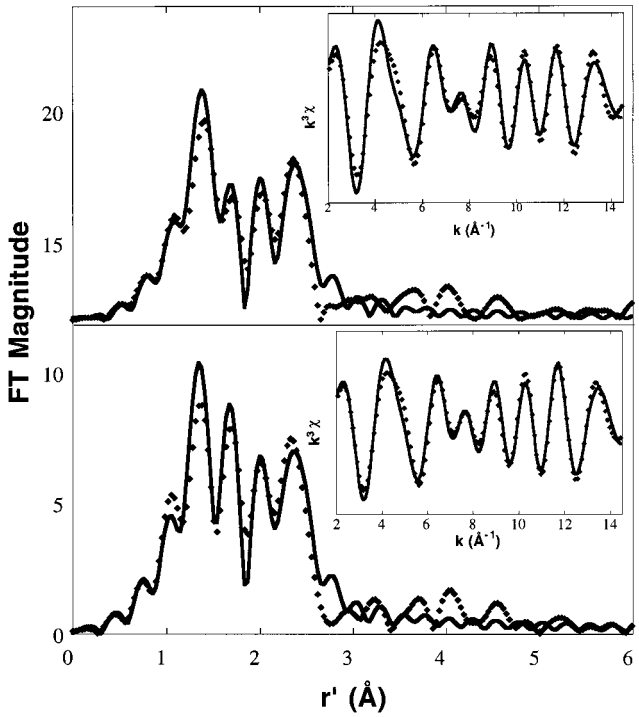

Figure 4. Fourier transforms and back-transforms (insets) of EXAFS data of $[Fe_2(\mu\text{-}O)_2(5\text{-}Et_3\text{-}TPA)_2][ClO_4]_3$ (**2**) (top; Table 5, fit 8) and $[Fe_2(\mu\text{-}O)_2(5\text{-}Me_3\text{-}TPA)_2][ClO_4]_3$ (**3**) (bottom; Table 5, fit A): experimental data (dots), simulation (solid line).

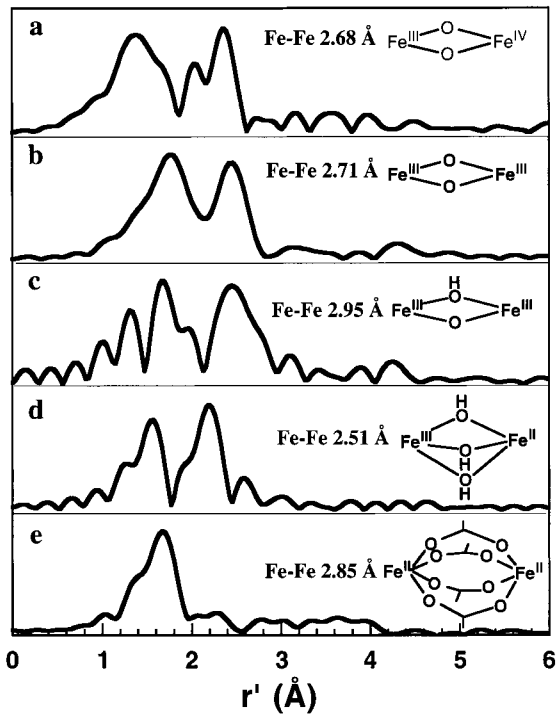

Figure 5. EXAFS spectra for crystallographic characterized diiron complexes with short Fe−Fe distances: (a) $[Fe_2(\mu\text{-}O)_2(5\text{-}Et_3\text{-}TPA)_2]^{3+}$; (b) $[Fe_2(\mu\text{-}O)_2(6\text{-}Me_3\text{-}TPA)_2]^{2+}$; (c) $[Fe_2(\mu\text{-}O)(\mu\text{-}OH)(6\text{-}Me_3\text{-}TPA)_2]^{3+}$; (d) $[Fe_2(\mu\text{-}OH)_3(Me_3TACN)_2]^{2+}$; (e) $[Fe_2(O_2CCMe_3)_4(Py)_2]$.

in the oxygen evolving complex of photosystem II and Mn-catalase in the superoxidized form[31] as well as in biomimetic copper−oxygen chemistry.[27e] Figure 5 illustrates that intense second-sphere features are also a characteristic of diiron

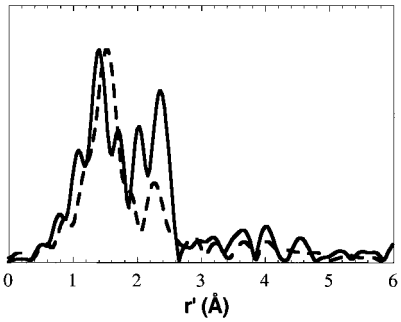

Figure 6. Fourier transformed EXAFS spectra of $[Fe_2(\mu\text{-}O)_2(5\text{-}Et_3\text{-}TPA)_2][ClO_4]_3$ (**2**) (solid line) and $[Fe(5\text{-}Me_3\text{-}TPA)(acac)][ClO_4]_2$ (dashed line).

complexes having short Fe−Fe distances with at least two single atom bridges. Thus the backscattering from the second iron is easily observed for $[Fe_2(\mu\text{-}O)_2(6\text{-}Me_3\text{-}TPA)_2]^{2+}$ (2.71 Å),[10] $[Fe_2(\mu\text{-}O)(\mu\text{-}OH)(6\text{-}Me_3\text{-}TPA)_2]^{3+}$ (2.95 Å),[32] and $[Fe_2(\mu\text{-}OH)_3(Me_3\text{-}TACN)_2]^{2+}$ (2.51 Å),[33] but not for $[Fe_2(\mu\text{-}O_2CC(CH_3)_3)_4(py)_2]$ (2.85 Å).[34] These observations emphasize the notion that the second-sphere feature becomes intense only in complexes with more rigid core structures.

In our earlier EXAFS analysis of **3**, we associated the outer-sphere features with an Fe scatterer at 2.89 Å.[12] Such a distance is clearly inconsistent with the crystal structure of **2**. In the current study, the best fit for the outer-sphere features consists of subshells of 1 Fe at 2.61 Å and 7−8 C at 2.87 Å (fits 8 and 9). Fits 5−9 in Table 5 summarize our various attempts to fit the outer sphere. When only a single shell is used, an Fe scatterer at 2.92 Å still affords the lower residual over a multiccarbon shell at a comparable distance (fit 5 vs fit 6). However, the goodness-of-fit improves significantly when Fe and C shells at 2.61 and 2.87 Å, respectively, are included (fit 8). When the Fe and C shells are interchanged (fit 7), the ϵ^2 value doubles. We have also analyzed EXAFS data for two samples of **3**, $[Fe_2(O)_2(5\text{-}Me_3\text{-}TPA)_2](ClO_4)_3$, by following the above protocol. The best fits for each sample listed in Table 5 demonstrate the reproducibility of the model derived from the EXAFS analysis of **2**. (Detailed fitting results for **3** are provided in Tables S6 and S7 in the Supporting Information.)

Our earlier reported EXAFS analysis of **3** overestimated the Fe−Fe distance by 0.2 Å. This result was a consequence of our failure to include the multi-carbon shell at 2.87 Å in the analysis. The required inclusion of this shell appears to be a feature of low-spin Fe(TPA) complexes. Examination of the crystal structures of such complexes shows that there are six carbon scatterers at 2.8−2.9 Å (r_{av} 2.86 Å) arising from the CH_2 and α-pyridyl carbons. Similarly, the EXAFS spectrum of the low-spin iron(III) complex, $[Fe(5\text{-}Me_3\text{-}TPA)acac]^{2+}$ (Figure 6), exhibits a prominent outer-sphere feature that can be fit with a multi-carbon shell at 2.83 Å (Table S8), in agreement with the average Fe−C distance of 2.84 Å determined from X-ray crystallography.[26] However, the inclusion of a multi-carbon shell is not required to obtain accurate Fe−Fe distances in the EXAFS analysis of high-spin complexes such as $[Fe_2(O)_2(6\text{-}Me_3\text{-}TPA)_2](ClO_4)_2$ and $[Fe_2(O)(OH)(6\text{-}Me_3\text{-}TPA)_2](ClO_4)_3$. The intensity of this multi-carbon shell in low-spin Fe(TPA) complexes is

(32) Zang, Y.; Pan, G.; Que, L., Jr.; Fox, B. G.; Münck, E. *J. Am. Chem. Soc.* **1994**, *116*, 3653−3654.

(33) (a) Drüeke, S.; Chaudhuri, P.; Pohl, K.; Wieghardt, K.; Ding, X.-Q.; Bill, E.; Sawaryn, A.; Trautwein, A. X.; Winkler, H.; Gurman, S. J. *J. Chem. Soc., Chem. Commun.* **1989**, 59−62. (b) Gamelin, D. R.; Bominaar, E.; Kirk, M. L.; Wieghardt, K.; Solomon, E. I. *J. Am. Chem. Soc.* **1996**, *118*, 8085−8097.

(34) Randall, C. R.; Shu, L.; Chiou, Y.-M.; Hagen, K. S.; M. Ito, N. K.; Lachicotte, R. J.; Zang, Y.; Que, L., Jr. *Inorg. Chem.* **1995**, *34*, 1036−1039.

Table 6. Deduced Fe−Fe Distances (Å) for **2**, MMOH-**Q**, and RNR R2-**X** with Fe Fitting Parameters Extracted from Different Complexes

fit standard model	**2**	MMOH-**Q**	RNR R2-**X**
$[Fe_2(\mu\text{-}O)(\mu\text{-}OH)(6\text{-}Me_3\text{-}TPA)_2]^{3+}$	2.61	2.47	2.49
$[Fe_2(\mu\text{-}OH)_3(Me_3\text{-}TACN)_2]^{2+}$	2.62	2.49	2.50
$[Fe_2(\mu\text{-}O)_2(6\text{-}Me_3\text{-}TPA)_2]^{2+}$ (**1**)	2.66	2.51	2.53
$[Fe_2(\mu\text{-}O)_2(5\text{-}Et_3\text{-}TPA)_2]^{3+}$ (**2**)		2.52	2.54

probably due to the increased rigidity of the metal−ligand bonds and the similarity of the Fe−C distances that allow their contributions to combine constructively to produce an intense outer-sphere feature. The results of this analysis demonstrate some of the limitations of the EXAFS method when insufficient information is available to allow exploration of the entire fitting hyperspace.

The 2.61 Å Fe−Fe distance associated with **2** in the EXAFS analysis reported here underestimates the crystallographically determined Fe−Fe distance by 0.07 Å, a discrepancy larger than normally associated with such analyses. Such errors are usually minimized by using fitting parameters (the amplitude reduction factor *A* and the energy shift ΔE) extracted from crystallographically determined model complexes of like structure. For our analysis we have used parameters extracted from the closely related $[Fe_2(O)(OH)(6\text{-}Me_3\text{-}TPA)_2](ClO_4)_3$. With fitting parameters for an Fe scatterer extracted from $[Fe_2(O)_2(6\text{-}Me_3\text{-}TPA)_2](ClO_4)_2$ and $[Fe_2(\mu\text{-}OH)_3(Me_3TACN)_2]^{2+}$ as standards, fits of **2** afforded Fe−Fe distances of 2.66 and 2.62 Å, respectively (Table 6), illustrating the axiom that more accurate fits are obtained as the model used approaches the structure of the unknown. These results provide a way to assess the uncertainties for the Fe−Fe distances deduced for MMOH-**Q** and RNR R2-**X** by EXAFS analysis (vide infra).

Implications for the Structures of MMOH Intermediate Q and RNR R2 Intermediate X. Compound **2** represents the first structurally characterized bis(μ-oxo)diiron complex with a formal $Fe^{III}Fe^{IV}$ oxidation state. Its existence emphasizes the notion that high-valent diiron species can be accessed by an $M_2(\mu\text{-}O)_2$ diamond core motif and is very likely stabilized by the two oxo bridges as precedented in high-valent manganese and copper chemistry.[9] Notably, **2** and related complexes have properties that closely resemble those of high-valent intermediates **Q** and **X** in the MMOH and RNR R2 redox cycles, respectively.[8] This resemblance has led to the suggestion that MMOH-**Q** and RNR R2-**X** may have similar core structures.

A key technique for the structural characterization of MMOH-**Q** and RNR R2-**X** is EXAFS. Since the likelihood of obtaining X-ray crystallographic information on these unstable species appears quite low at present, EXAFS represents an alternative approach to obtain metrical details of the iron coordination environment. EXAFS analysis of MMOH-**Q** and RNR R2-**X** has revealed the presence of low-*Z* shells at 1.8 and 2.0 Å and an Fe shell at 2.5 Å, very similar to what is observed for **2**.[5,6] The 2.0 Å shell represents the histidine and carboxylate ligands and differs little from corresponding shells in the diiron(II) and diiron(III) forms of these enzymes. The 1.8 Å shell is best simulated by one short Fe−O bond, typically associated with an oxo bridge. Thus the core structures of MMOH-**Q** and RNR R2-**X** minimally consist of (μ−oxo)diiron units. However, an $Fe_2(\mu\text{-}O)_2$ diamond core is not precluded, since the two Fe−μ-O bonds of **2** (1.80 and 1.86 Å) appear as only one scatterer at 1.83 Å in the EXAFS analysis and cannot be fit well as a two-scatterer shell, presumably due to destructive interference with each other and with the 2.0 Å shell (vide supra).

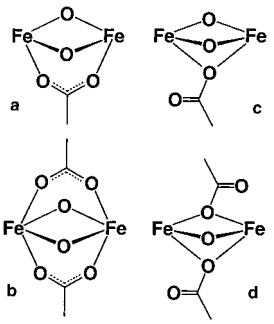

Figure 7. Possible core structures for MMOH-**Q** and RNR R2-**X**.

The short Fe−Fe distance of ca. 2.5 Å found for MMOH-**Q** and RNR R2-**X** requires the presence of at least two single-atom bridges. Table 6 lists the Fe−Fe distances obtained for MMOH-**Q** and RNR R2-**X** using Fe fitting parameters derived from a number of crystallographically characterized diiron complexes including **2** and shows that the Fe−Fe distances hover around 2.5 Å within an acceptable error range. The Fe−Fe distance of 2.68 Å now crystallographically established for **2** is at least 0.15 Å longer than those found for MMOH-**Q** and RNR R2-**X**, suggesting that an $Fe_2(\mu\text{-}O)_2$ diamond core structure alone is insufficient to afford an Fe−Fe separation of 2.5 Å. We have proposed the need for at least one other bridge to shorten the Fe−Fe distance.[5,6] It has been demonstrated that the addition of a bidentate carboxylate bridge shortens the M−M distance of an $Mn_2(\mu\text{-}O)_2$ core by 0.1 Å (Figure 7a).[35] More recently, it has been found that the addition of two bidentate carboxylate bridges contracts the metal−metal distance in a complex with an $Fe_2(\mu\text{-}OH)_2$ core by at least 0.2 Å.[36] The involvement of such a bridge is quite likely, since one bidentate carboxylate bridge (E144 in MMO and E115 in RNR R2) is a common feature of all the available crystal structures of these two enzymes.[37,38] Indeed such a triply bridged structure is also predicted by density function theory calculations.[39] A second bidentate carboxylate bridge may also be involved to achieve the 2.5 Å distance (Figure 7b); this bridge would likely then correspond to E243 of MMO and E238 of RNR R2, which act as bridges to the diiron(II) centers of these enzymes.[37b,38c]

Alternatively, a core structure with three single-atom bridges can also afford a 2.5 Å Fe−Fe separation, as precedented by the mixed valence complex $[Fe_2(\mu\text{-}OH)_3(Me_3TACN)_2]^{2+}$ (Fe−Fe 2.51 Å).[32] Besides an oxo group, the most likely candidate for an additional bridge is one of the carboxylate ligands in the

(35) (a) Haselhorst, G.; Wieghardt, K. *J. Inorg. Biochem.* **1995**, *59*, 624. (b) Pal, S.; Gohdes, J. W.; Wilisch, W. C. A.; Armstrong, W. H. *Inorg. Chem.* **1992**, *31*, 713−716. (c) Dave, B. C.; Czernuszewicz, R. S.; Bond, M. R.; Carrano, C. J. *Inorg. Chem.* **1993**, *32*, 3593−3594.

(36) Lee, D.; Lippard, S. J. *J. Am. Chem. Soc.* **1998**, *120*, 12153−12154.

(37) (a) Rosenzweig, A. C.; Frederick, C. A.; Lippard, S. J.; Nordlund, P. *Nature* **1993**, *366*, 537−543. (b) Rosenzweig, A. C.; Nordlund, P.; Takahara, P. M.; Frederick, C. A.; Lippard, S. J. *Chem. Biol.* **1995**, *2*, 409−418. (c) Elango, N.; Radhakrishnan, R.; Froland, W. A.; Wallar, B. J.; Earhart, C. A.; Lipscomb, J. D.; Ohlendorf, D. H. *Protein Sci.* **1997**, *6*, 556−568.

(38) (a) Nordlund, P.; Sjöberg, B.-M.; Eklund, H. *Nature* **1990**, *345*, 393−398. (b) Nordlund, P.; Eklund, H. *J. Mol. Biol.* **1993**, *232*, 123−164. (c) Logan, D. T.; Su, X.-D.; Åberg, A.; Regnström, K.; Hajdu, J.; Eklund, H.; Nordlund, P. *Structure* **1996**, *4*, 1053−1064. (d) Logan, D. T.; deMaré, F.; Persson, B. O.; Slaby, A.; Sjöberg, B. M.; Nordlund, P. *Biochemistry* **1998**, *37*, 10798−10870.

(39) Siegbahn, P. E. M.; Crabtree, R. H. *J. Am. Chem. Soc.* **1997**, *119*, 3103−3113.

(40) (a) Burdi, D.; Sturgeon, B. E.; Tong, W. H.; Stubbe, J.; Hoffman, B. M. *J. Am. Chem. Soc.* **1996**, *118*, 281−282. (b) Willems, J.-P.; Lee, H.-I.; Burdi, D.; Doan, P. E.; Stubbe, J.; Hoffman, B. M. *J. Am. Chem. Soc.* **1997**, *119*, 9816−9824. (c) Burdi, D.; Willems, J.-P.; Riggs-Gelasco, P.; Antholine, W. E.; Stubbe, J.; Hoffman, B. M. *J. Am. Chem. Soc.* **1998**, *120*, 12910−12919.

active site, undergoing yet another carboxylate shift when the active site accesses the high-valent state (Figure 7c,d). Figure 7d is favored for RNR R2-**X** in light of ENDOR evidence for only one oxo bridge.[40] To date, however, there are no synthetic high-valent metal complexes with a combination of ligating groups as proposed in Figure 7d, although examples of monodentate carboxylate bridges have been found in diiron(II) and diiron(III) complexes.[41]

In conclusion, we have crystallized $[Fe_2(\mu\text{-}O)_2(5\text{-}Et_3\text{-}TPA)_2](ClO_4)_3$ (**2**) and characterized its novel $Fe^{III}Fe^{IV}(\mu\text{-}O)_2$ diamond core structure. Analysis of the EXAFS data for **2** reveals features with distances in excellent agreement with the crystallographic data. Complex **2** serves as a model for the high-valent diiron cores of MMOH-**Q** and RNR R2-**X**. The fact that MMOH-**Q** and RNR R2-**X** have a set of EXAFS features quite similar to those of **2** supports the notion that an $Fe_2(\mu\text{-}O)_2$ core may be utilized to access high-valent states in the oxygen activation cycles of these nonheme diiron enzymes.

(41) (a) Tolman, W. B.; Bino, A.; Lippard, S. J. *J. Am. Chem. Soc.* **1989**, *111*, 8522−8523. (b) LeCloux, D. D.; Barrios, A. M.; Mizoguchi, T. J.; Lippard, S. J. *J. Am. Chem. Soc.* **1998**, *120*, 9001−9014. (c) Spartalian, K.; Bonadies, J. A.; Carrano, C. J. *Inorg. Chim. Acta* **1988**, *152*, 135−138.

Acknowledgment. This work was supported by the National Institutes of Health (GM-38767). The National Science Foundation provided funds for the purchase of the Siemens SMART system. Beamline X9 of the National Synchrotron Light Source at Brookhaven National Laboratory is supported by the National Institutes of Health (RR-001633).

Supporting Information Available: Tables S1−S5 of the crystallographic experimental details, the atomic coordinates, thermal parameters, bond lengths, and bond angles for $[Fe_2(\mu\text{-}O)_2(5\text{-}Et_3\text{-}TPA)_2](ClO_4)_3$ (**2**), Tables S6 and S7 of EXAFS fits for $[Fe_2(O)_2(5\text{-}Me_3\text{-}TPA)_2](ClO_4)_3$ (**3**), Table S8 of EXAFS fits for $[Fe(5\text{-}Me_3\text{-}TPA)(acac)](ClO_4)_2$ and a thermal ellipsoid (Figure S1) for $[Fe_2(\mu\text{-}O)_2(5\text{-}Et_3\text{-}TPA)_2](ClO_4)_3$ (**2**) (PDF). An X-ray crystallographic file, in CIF format, is available. This material is available free of charge via the Internet at http://pubs.acs.org.

JA983666Q